

# Microwave Backscatter Over Greenland: Changing With Time

Ivan S. Ashcraft and David G. Long

Brigham Young University Microwave Earth Remote Sensing Laboratory,  
459 Clyde Bulding, Provo, UT 84602

## ABSTRACT

Changes in the Greenland ice sheet are considered important indicators of global climate change. These changes can be monitored using space-borne scatterometers which provide frequent coverage of the entire ice sheet. This paper provides a general overview of backscatter measurements over Greenland and the distinguishing attributes of the data sets over the different snow facies including temporal signatures. Seasat-A scatterometer (1978), NSCAT (1996-1997), SeaWinds (1999-present), and ERS AMI (1992-2000) scatterometer data are analyzed to evaluate the long term changes in the ice sheet. An increase in backscatter is observed in the dry snow zone near the dry snow zone/percolation zone boundary. A simple algorithm is applied to determine the length and extent of the melt for the summer of 1999 as observed by SeaWinds and ERS. A comparison between the two sensors shows similar results with the apparent differences attributed to the higher temporal resolution of SeaWinds and the difference in frequencies between the two instruments.

**Keywords:** Greenland, scatterometry, snow, backscatter, radar scattering

## 1. INTRODUCTION

The Greenland ice sheet is considered an important measuring stick for climate change. Greenland is completely covered by snow and ice year round with the exception of a small area along the coastline. However, some summer surface melt occurs over a significant portion of the ice sheet periphery. The balance between accumulation and ablation is a critical indicator of potential global climate change.

Greenland is a vast, mostly uninhabited island. Various ground stations have been established which provide valuable in-situ measurements. However, these ground stations only provide limited coverage of the ice sheet. Thus there is a strong interest in remotely sensing changes in the ice sheet. Microwave instruments are effective in monitoring the ice sheet because of their sensitivity to the presence of liquid melt water in the snow pack and to the roughness of the snow surface. Microwave measurements are also immune to effects of cloud cover and solar illumination making measurements possible for day and night coverage during all weather conditions. Air-borne and Space-borne synthetic aperture radar (SAR) can provide high resolution data, but the coverage is limited and usually. Wind scatterometers collect data at much lower resolution than SAR, but give complete coverage within days. NASA's SeaWinds scatterometer covers the entire ice sheet twice daily. Because of the frequent large scale coverage, scatterometer data sets can provide important information about the dynamic behavior of the ice sheet.

In this paper we give a brief background on the scatterometer data sets used, discuss the defining attributes of the different Greenland ice facies, show changes in the microwave backscatter over Greenland in the past quarter of a century, and demonstrate how scatterometer measurements can be used to track the extent and duration of the Greenland summer melt.

## 2. SCATTEROMETER BACKGROUND

Wind scatterometers are primarily designed for measuring vector wind speeds over the ocean. In order to determine the wind speed, the scatterometer measures the normalized radar backscatter cross section ( $\sigma^o$ ). These measurements are collected over land, ice, and water. In recent years, these  $\sigma^o$  measurements have been used effectively in many land/ice studies.<sup>1-4</sup>

The scatterometer data sets used in this paper come from two basic scatterometer system designs. The designs are not discussed in great detail here, but there are some fundamental differences which lead to fundamental differences

---

Correspondence: I.S.A.: E-mail: ashcraft@ee.byu.edu

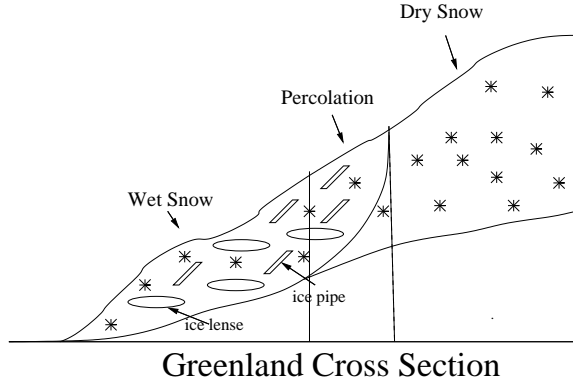


**Figure 1.** Cross section of the Greenland ice sheet.

in the data sets. A fan-beam scatterometer uses multiple long and narrow antennas, each illuminating a long narrow area on the Earth’s surface. The return from each antenna footprint is subdivided using range filtering such that there are multiple measurements, each at a different incidence angle. Thus, the data set consists of  $\sigma^o$  measurements at a range of incidence angles. Fan-beam scatterometers used in this study include the Seasat-A scatterometer (SASS), the NASA Scatterometer (NSCAT) and the ERS-1 and ERS-2 Advanced Microwave Instrument (AMI) hence forth ERS. A pencil-beam scatterometer has a conically scanning dish providing a large range for azimuth coverage, but only one incidence angle. Data from NASA’s SeaWinds on QuikSCAT, which has a pencil-beam design, are used extensively in this paper.

An effective method for utilizing  $\sigma^o$  measurements over land and ice is to create  $\sigma^o$  images. For fan-beam scatterometers, the incidence angle dependence of the data is accounted for using the model

$$\sigma^o(\theta) = A + B(\theta - \theta_{\text{ref}})$$

where  $\sigma^o$  is measured in dB,  $\theta$  is the incidence angle,  $\theta_{\text{ref}}$  is a reference incidence angle,  $A \approx \sigma^o(\theta_{\text{ref}})$ , and  $B$  gives the dependence of  $\sigma^o$  on  $\theta$ .  $A$  and  $B$  are adjusted to best fit the model to the data. For the pencil beam scatterometer, only  $A$  can be determined and  $\theta_{\text{ref}}$  is equal to the incidence angle of the antenna beam. Images of  $A$  and  $B$  over the region of interest can be used for analysis. Not only are the images effective for visual analysis, but by using the Scatterometer Reconstruction Algorithm<sup>5,6</sup> (SIR) to generate the image, the resolution of the image is higher than the resolution of the original raw data measurements. Because the SIR algorithm requires multiple passes, with the possible exception of SeaWinds, it is necessary to assume it minimal temporal change during the imaging interval. During the winter this assumption is valid, but during the summer, this assumption can result in averaging the rapid changes associated with a melt event.

### 3. BACKSCATTER SIGNATURE OF DIFFERENT ICE FACIES

The Greenland ice sheet consists of multiple ice facies<sup>1</sup> as illustrated in Fig. 1. The facies type is determined by the state of the snow at the peak summer melt. The dry snow zone is defined as the region in which the snow never melts ( $T < -10^\circ\text{C}$  year round). Because there is little change in the surface characteristics,  $\sigma^o$  is minimal variation and is dominated by volume scattering. At lower altitudes, the higher temperatures increase the vapor pressure of ice ultimately leading to an increase in snow grain-size. Also when the temperature increases sufficiently for liquid water to form, it percolates downward preferentially in pipes or channels. When the water refreezes the result is ice structures referred to as ice pipes or lenses. This region is termed the percolation zone. If the top meter or more of snow has liquid water present (isothermal at  $0^\circ\text{C}$ ) then the region is referred to as the wet snow zone. The region in which the snow melts entirely leaving a bare ice surface is termed the ablation zone.

The key to monitoring Greenland is understanding the backscatter response of the different snow zones. There are two basic keys to understanding the backscatter response at C-band and Ku-band for off nadir incidence angles. First, the presence of liquid water significantly reduces  $\sigma^o$ . Second, the grain growth and ice structure formation caused by the melt/refreeze cycle contribute to an increase in backscatter compared to dry snow. A more detailed discussion

of the  $\sigma^o$  values observed over Greenland is given in 1. Figure 2 (a) shows five  $\sigma^o$  images of Greenland created from SeaWinds data. These images span the summer of 2000 Greenland melt cycle. Each image was produced using 1 day of vertical polarization  $\sigma^o$  measurements. The images have 4.5 km pixel resolution with a nominal resolution of approximately 10 km. The notable characteristics in these images are

- low values of  $\sigma^o$  along the periphery of the ice-sheet during the peak melt indicating the presence of liquid water,
- a band of high values of  $\sigma^o$  some distance inland from the ice-sheet periphery indicating frozen subsurface ice structures,
- the dramatic change from high to low  $\sigma^o$  values and then back as the melt occurs around the edge of the ice sheet, and
- a region of lower  $\sigma^o$  values in the center portion of Greenland corresponding to the dry snow.

The plots shown in Fig. 2 (b) and (c) show time series of the  $\sigma^o$  measurements at the two points indicated on Fig. 2 (a). The location for Fig. 2 (b) is located in the percolation zone near the edge of the dry snow zone and for Fig. 2 (c) it is in the wet snow zone. These time-series plots show the sharp decrease in backscatter that occurs during a melt event. This decrease can be used to identify the duration and extent of the melt as discussed in Sect. 5.

#### 4. CHANGES IN BACKSCATTER OVER TIME

In order to understand the significance of the changes occurring on the Greenland ice sheet, it is important to observe the changes over a long time period. The ERS data set is the longest continuous scatterometer data set available, spanning from 1992 to 2000. Also, SASS, NSCAT, and SeaWinds can be combined to observe the net change over 22 years. Because of the difference in frequency, the  $\sigma^o$  values from ERS and the other sensors are not compared directly.

The sharp contrast between the  $\sigma^o$  signature of the dry snow zone and the percolation zone make it possible to observe the lateral movement of the dry snow zone/percolation zone boundary by comparing  $\sigma^o$  images from year to year. As previously noted, the large snow grain size and subsurface ice structures contribute to high backscatter measurements from the percolation zone, whereas the dry snow zone has much lower  $\sigma^o$  values. Figure 3 shows changes in  $\sigma^o$  at C-band as measured by the ERS scatterometer. The images on the upper left and bottom right are ERS *A* images from Julian Day (J.D.) 331-360, 1992 and 2000 respectively. The other images show the difference between an *A* image from the same period of a following year and the 1992 original image. Thus the sequence of images gives a time series of the cumulative changes since 1992. By 2000 there are significant changes, mostly along the dry snow zone/percolation zone boundary. The major difference is a  $\sigma^o$  increase of over 4 dB over a significant area of the upper part of the percolation zone, and as much as a 3 dB decrease in  $\sigma^o$  around the edge of the dry snow zone. This suggests an upslope movement of the dry snow zone/percolation zone boundary which is consistent with increased warming.

The time-series plot in Fig. 3 (b) shows the backscatter at 71.39° N 46.21° W which location is indicated by a “+” on each image in Fig. 3 (a). The backscatter at this location is relatively constant from 1992 to mid-summer 1997. At this point there is an abrupt 7 dB rise in  $\sigma^o$ . The jump is attributed to a melt event, although the large decrease in  $\sigma^o$  that is typical of a melt event is not observed in the data. The reasoning behind this is that in this location a melt event would be very short and easily filtered out by the four day imaging interval used in obtaining the data. From the summer of 1997 to the summer of 2000 there is a linear decrease in  $\sigma^o$  of  $\sim 2$  dB which can be attributed to accumulation.<sup>7</sup>

Similar results are observed for Ku-band as shown in Fig. 4. The figure includes 4 images. The left image is from SASS using data from J.D. 249-278, 2000. The next image to the right shows the difference between NSCAT (J.D. 270-275, 1996) and the original SASS. This image shows significant increase in  $\sigma^o$  along the dry snow zone/percolation zone boundary between 1978 and 1996. Following is the difference between SeaWinds (J.D. 271-273, 2000) and SASS. Further increase in  $\sigma^o$  is observed. Finally, image furthest to the right is the original SeaWinds image showing the backscatter values after the change. The changes are very similar to those observed for the C-band ERS data.

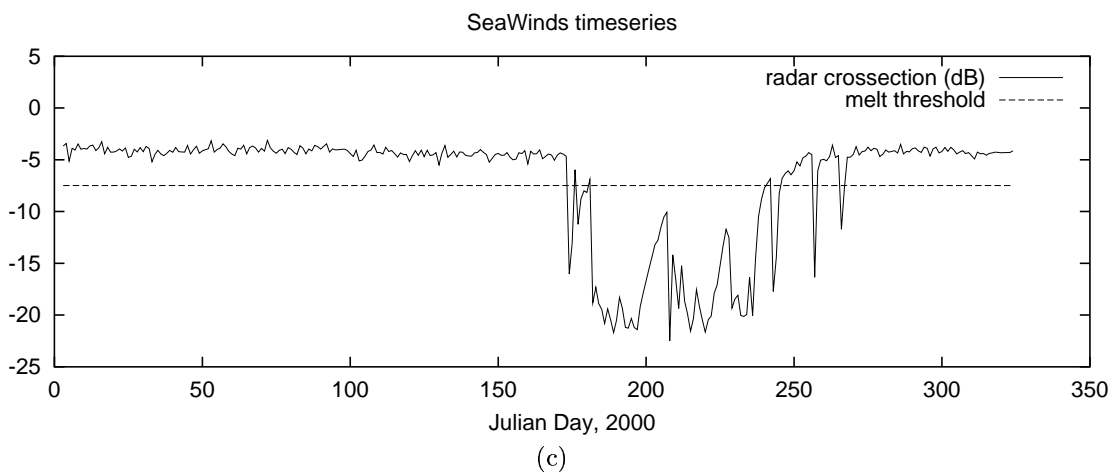
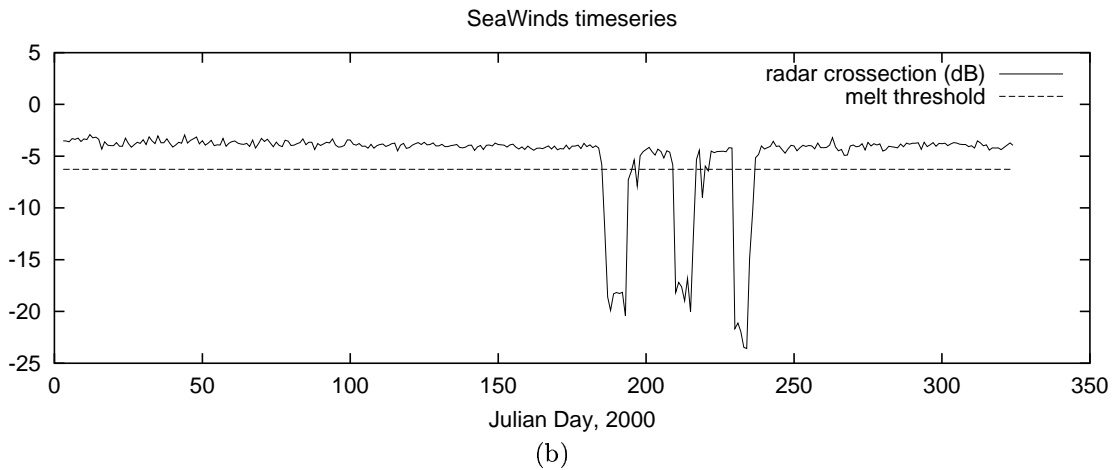
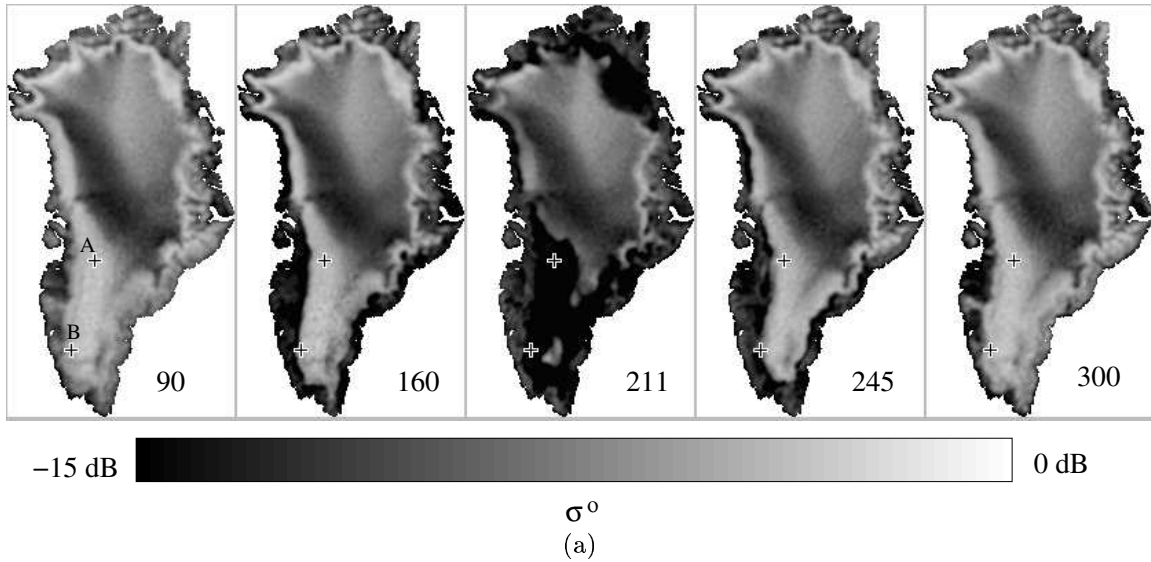
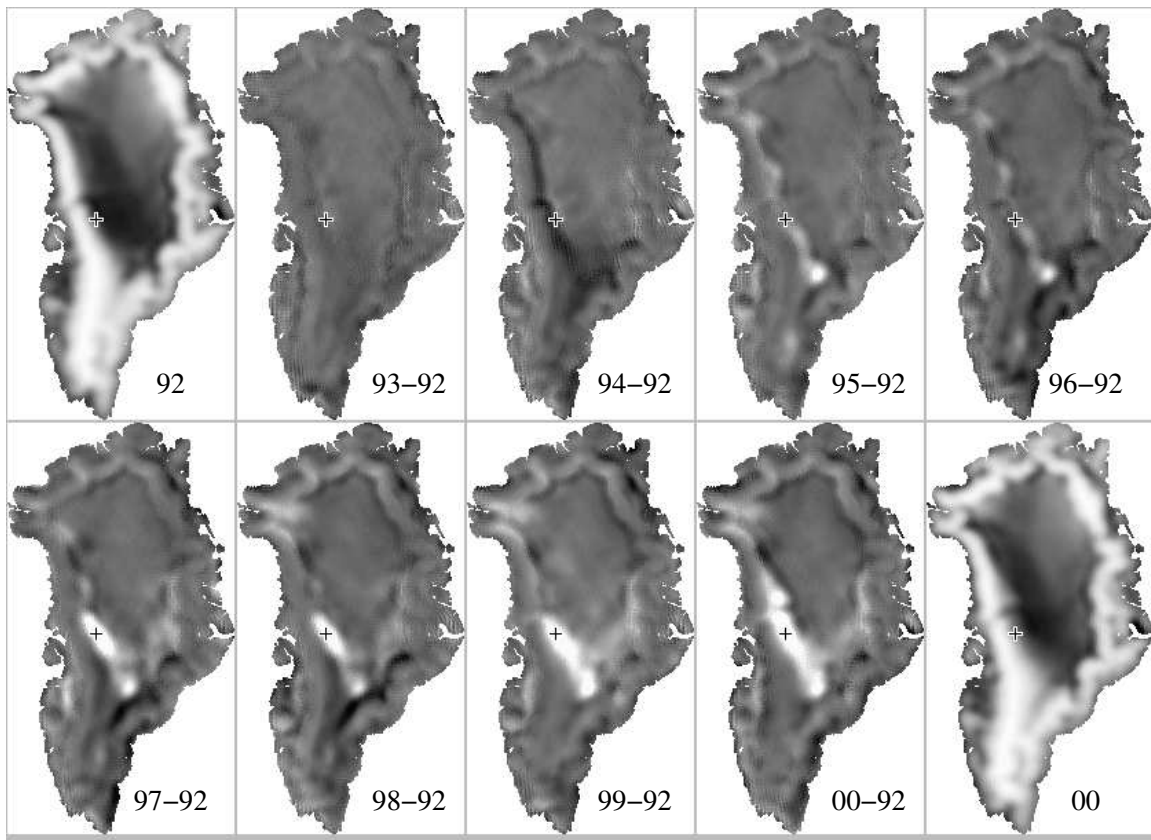
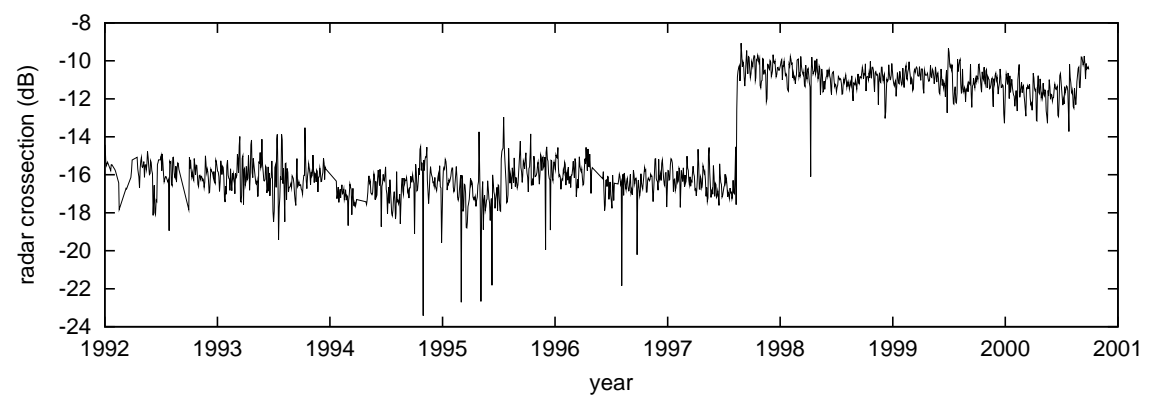


**Figure 2.** (a) An image time-series showing the summer melt over Greenland during 2000 as observed by SeaWinds on QuikSCAT. The Julian Day is indicated on each image. (b) and (c) are time series plots from SeaWinds for the points A and B respectively in (a). Point A is located at 68.85° N 45.83° W and point B is at 63.54° N 48.34° W.



(a)



(b)

**Figure 3.** (a) ERS  $\sigma_v^o(40^\circ)$  images and difference images showing changes on the Greenland ice sheet between 1992 and 2000. (b) C-band  $\sigma_v^o(40^\circ)$  measured by ERS at  $71.39^\circ$  N  $46.21^\circ$  W from 1992 to 2000. The location is indicated by a “+” in the images in (a).

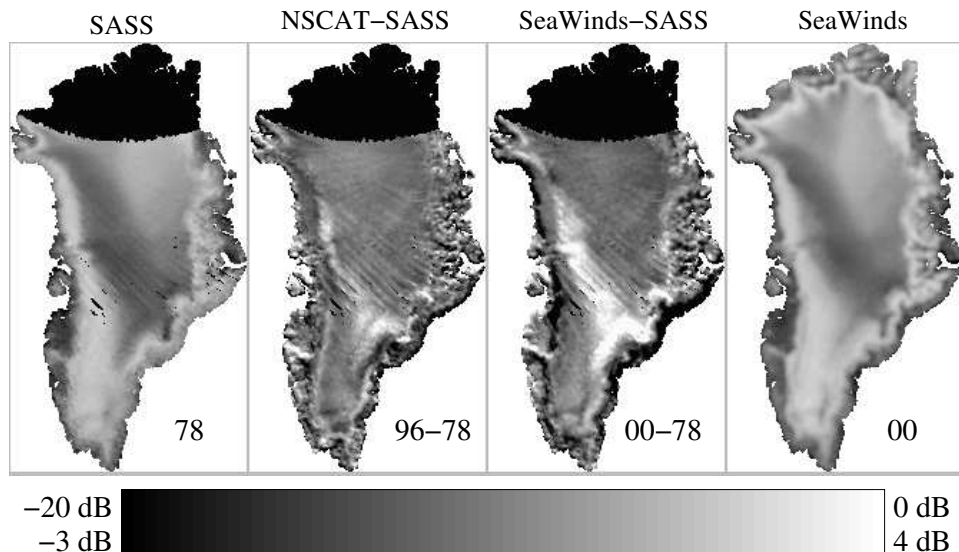


**Figure 4.** Images of the change in  $\sigma_v^o(54.1^\circ)$  at Ku-band. The left and right images are from SASS and SeaWinds. The inner two images the difference between NSCAT and SASS, and SeaWinds and SASS.

## 5. MELT EXTENT AND DURATION

The presence of liquid water in the snow pack causes a sharp drop in  $\sigma^o$ . This makes scatterometers nearly ideal for observing the melt extent and duration during the Greenland summer. SeaWinds is particularly well suited having complete twice daily coverage. A simple algorithm for identifying a melt event<sup>8</sup> is to define a threshold value ( $\sigma_{\text{melt}}^o$ ) so that a melt event is flagged if  $\sigma^o < \sigma_{\text{melt}}^o$ . Because of the magnitude of the drop in  $\sigma^o$  during a melt, the algorithm is only mildly sensitive to the threshold value chosen. The chosen threshold used is

$$\sigma_{\text{melt}}^o = \mu_{\text{winter}} - 8\sigma_{\text{winter}}$$

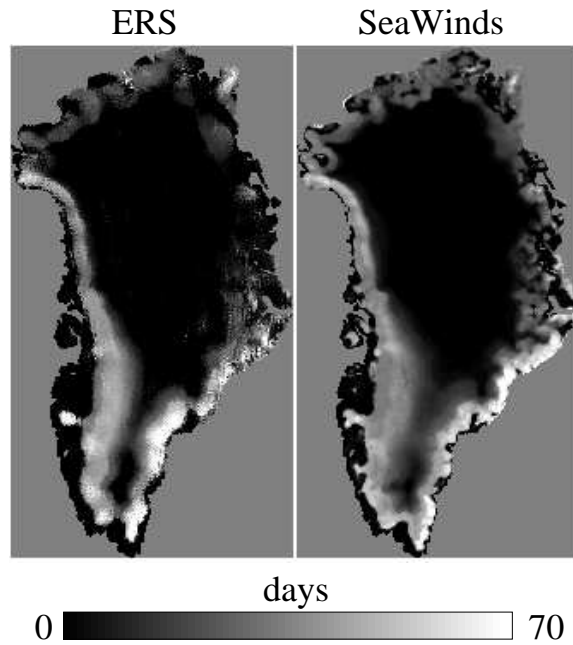
where  $\mu_{\text{winter}}$  and  $\sigma_{\text{winter}}$  are the mean and standard deviation respectively of  $\sigma^o$  for each pixel during the Greenland winter. For the purpose of this algorithm the winter is defined as the first 36 and final 36 days of the Julian year. The melt threshold calculated using this algorithm is included in the time-series plots shown in Fig. 2 (b) and (c).

Figure 5 shows the duration of the summer 1999 melt calculated by from ERS and SeaWinds data. Because SeaWinds data is not available prior to J.D. 201, 1999, the melt for both sensors is calculated beginning with this date. The SeaWinds data is from only descending (evening) passes which show the largest melt extent. The longest melt observed by both sensors is around 70 days and occurs on the edge of the ice sheet. In the percolation zone there is a steep gradient in the melt duration showing reductions in the length of the melt. SeaWinds observes melt further inland than ERS which is partially attributed to the fact that SeaWinds can observe single day melt events and the difference in the time of day between the ERS and SeaWinds measurements. The ERS data used in this analysis is from 4 day images which include ascending and descending passes. The averaging tends to filter out 1 day melt events.

The extent of the melt over the ice sheet each day is shown in Fig. 6. The two sensors show very similar trends, though there is some difference in magnitude. During the peak melt SeaWinds observes a much larger melt area than ERS. This can be attributed in part to the higher temporal resolution of SeaWinds. SeaWinds also shows short melt events late in the year that are not observed by ERS. The similarities between the two sensors are promising for future combinations of the two data sets.

## 6. CONCLUSION

Scatterometers are effective tools for monitoring the Greenland ice sheet. They provide frequent complete coverage for all weather conditions. The large gradient in  $\sigma^o$  in the transition from the dry snow zone to the percolation zone



**Figure 5.** Melt duration after J.D. 200 during the summer of 1999. The image on the left is calculated from ERS data and the image on the right is from SeaWinds.

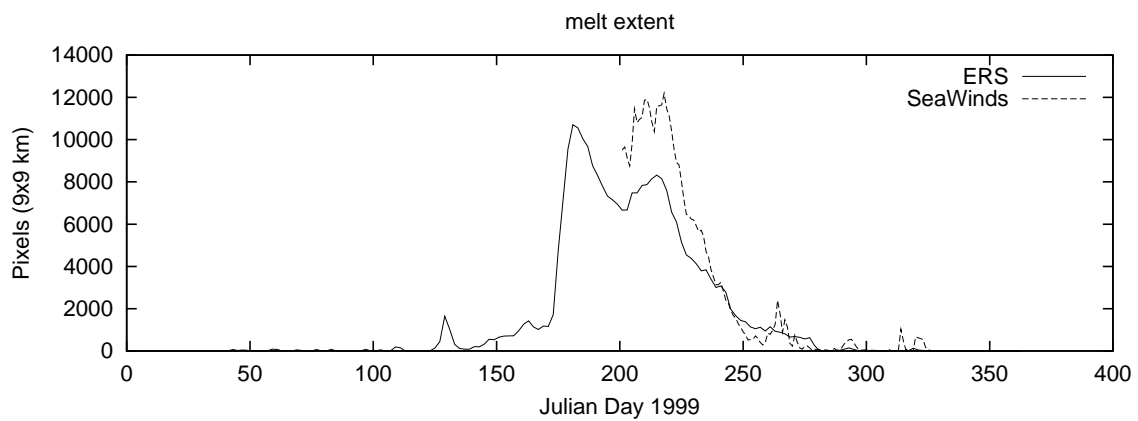


**Figure 6.** Melt extent each day for the summer of 1999 as calculated from ERS and SeaWinds data.

makes it possible to monitor lateral movements of this boundary over time. Scatterometer data records indicate an upslope movement of this boundary in recent years. The sensitivity of  $\sigma^o$  to the presence of liquid water in the snow pack make scatterometers ideal for monitoring the duration and extent of the summer melt over the Greenland ice sheet. Both SeaWinds and ERS are effective for tracking the melt, with SeaWinds having better than daily temporal resolution.

### ACKNOWLEDGMENTS

SeaWinds and ERS data were provided by the PO.DAAC at the Jet Propulsion Laboratory and the Scatterometer Climate Record Pathfinder at Brigham Young University (URL <http://www.scp.byu.edu/>).

### REFERENCES

1. D. G. Long and M. R. Drinkwater, "Greenland ice-sheet surface properties observed by the Seasat-A scatterometer at enhanced resolution," *J. of Glaciology* **40**(135), pp. 213–230, 1994.
2. M. R. Drinkwater, D. G. Long, and A. W. Bingham, "Greenland snow accumulation estimates from satellite radar scatterometer data," *Journal of Geophysical Research*, in press.
3. A. W. Bingham and M. R. Drinkwater, "Recent changes in the microwave scattering properties of the Antarctic ice sheet," *IEEE Trans. on Geosci. and Rem. Sens.* **38**(4), pp. 1810–1820, 2000.
4. N. Young, D. Hall, and G. Hyland, "Directional anisotropy of C-band backscatter and orientation of surface microrelief in East Antarctica," in *Proceedings of the First Australian ERS Symposium*, pp. 117–126, Feb. 1996.
5. D. G. Long, P. J. Hardin, and P. T. Whiting, "Resolution enhancement of spaceborne scatterometer data," *IEEE Trans. on Geosci. and Rem. Sens.* **31**(3), pp. 700–715, 1993.
6. D. S. Early and D. G. Long, "Image reconstruction and enhanced resolution imaging from irregular samples," *IEEE Trans. on Geosci. and Rem. Sens.* **39**(2), pp. 291–302, 2001.
7. V. Wismann, D. P. Winebrenner, K. Boehnke, and R. J. Arhern, "Snow accumulation on Greenland estimated from ERS scatterometer data," in *IEEE International Geoscience and Remote Sensing Symposium*, pp. 1823–1825, 1997.
8. I. S. Ashcraft and D. G. Long, "Seawinds views Greenland," in *IEEE International Geoscience and Remote Sensing Symposium*, 2000.